

Structural models of increasing complexity for icosahedral boron carbide with compositions throughout the single-phase region from first principles

A. Ektarawong,^{1,*} S. I. Simak,¹ and B. Alling^{1,2}

¹Theoretical Physics Division, Department of Physics, Chemistry and Biology (IFM), Linköping University, SE-581 83 Linköping, Sweden

²Max-Planck-Institut für Eisenforschung GmbH, Max-Planck Strasse 1, 40237 Düsseldorf, Germany



(Received 2 March 2018; published 18 May 2018)

We perform first-principles calculations to investigate the phase stability of boron carbide, concentrating on the recently proposed alternative structural models composed not only of the regularly studied $B_{11}C^p(\text{CBC})$ and $B_{12}(\text{CBC})$, but also of $B_{12}(\text{CBCB})$ and $B_{12}(\text{B}_4)$. We find that a combination of the four structural motifs can result in low-energy electron precise configurations of boron carbide. Among several considered configurations within the composition range of $B_{10.5}C$ and B_4C , we identify in addition to the regularly studied $B_{11}C^p(\text{CBC})$ at the composition of B_4C two low-energy configurations, resulting in a new view of the B-C convex hull. Those are $[B_{12}(\text{CBC})]_{0.67}[B_{12}(\text{B}_4)]_{0.33}$ and $[B_{12}(\text{CBC})]_{0.67}[B_{12}(\text{CBCB})]_{0.33}$, corresponding to compositions of $B_{10.5}C$ and $B_{6.67}C$, respectively. As a consequence, $B_{12}(\text{CBC})$ at the composition of $B_{6.5}C$, previously suggested in the literature as a stable configuration of boron carbide, is no longer part of the B-C convex hull. By inspecting the electronic density of states as well as the elastic moduli, we find that the alternative models of boron carbide can provide a reasonably good description for electronic and elastic properties of the material in comparison with the experiments, highlighting the importance of considering $B_{12}(\text{CBCB})$ and $B_{12}(\text{B}_4)$, together with the previously proposed $B_{11}C^p(\text{CBC})$ and $B_{12}(\text{CBC})$, as the crucial ingredients for modeling boron carbide with compositions throughout the single-phase region.

DOI: [10.1103/PhysRevB.97.174104](https://doi.org/10.1103/PhysRevB.97.174104)

I. INTRODUCTION

Boron carbide belongs to icosahedral boron-rich solids. Owing to its unusual bonding types, dominated by three-center two-electron bonds, the material possesses several prominent properties, e.g., high chemical and thermal stabilities, high hardness, high melting point, etc. The material is thus promising for various applications [1–7]. The crystal structure of boron carbide has mostly been described by 12-atom icosahedra, located at vertices of a rhombohedral unit cell ($R\bar{3}m$), and intericosahedral chains, filling the interstices between the icosahedra [8–11]. The icosahedron consist of two crystallographic sublattices, namely polar and equatorial sites. Each of them bonds to six neighboring icosahedra through the polar atoms, while each chain-end atom bridges the three surrounding icosahedra through the equatorial atoms.

Experimentally, boron carbide exhibits a single-phase solid solution over a relatively broad composition range, extending approximately from 8 to 20 at. % of C [1,7,12]. Thus a situation of B and C atoms to substitute for one another on the lattice sites within the single-phase region is conceivable. Inspection of the atomic configuration of the material at any given carbon content and temperature is, however, an outstanding challenge for both experimentalists and theoreticians. This is owing to its structural complexity as well as the similarities of B and C atoms in terms of the atomic form factors for x-ray diffraction [13] and of the nuclear scattering cross sections (^{11}B and ^{12}C) for neutron diffraction [11,14]. It should be

noted that the issues, regarding the solubility range [15–17] and atomic configuration [18–21] of boron carbide, have still been inconclusively debated.

Several first-principles studies [20–27] suggested two stable compositions of boron carbide, i.e., B_4C and $B_{6.5}C$ represented, respectively, by $B_{11}C^p(\text{CBC})$ [Fig. 1(a)] and $B_{12}(\text{CBC})$ [Fig. 1(b)], where the superscript p denotes the polar sublattice. However, these two configurations are not able to accurately provide a description of the material properties, as they result in large discrepancies between theoretical predictions and experimental observations. For example, boron carbide is known to be a semiconductor throughout the single-phase region [28,29], while first-principles calculations predict a metallic state for $B_{12}(\text{CBC})$ due to its electron deficiency [25,30,31]. Another example of the discrepancies is that the elastic and shear moduli of $B_{12}(\text{CBC})$ are severely underestimated, as compared to the experimental values [32]. Further detailed discussion of the discrepancies can be found elsewhere [20,21,33]. Recent theoretical studies [18–21,32] demonstrated that configurational disorder of B and C atoms, induced by high concentrations of low energy B/C substitutional defects, could be the reason for such discrepancies. Such disordered configurations of boron carbide were, however, predicted to be favored only at high temperature. Alternatively, Shirai *et al.* [33] initiated an idea of inclusion of $B_{12}(\text{B}_4)$ [Fig. 1(c)] with $B_{11}C^p(\text{CBC})$ and $B_{12}(\text{CBC})$ in modeling boron carbide within the single-phase region, together with its capability to compensate for the electron deficiency in $B_{12}(\text{CBC})$, and showed that such structural models are rather low in energy comparable to that of $B_{12}(\text{CBC})$. We note that the chain motif B_4 was originally proposed by Yakel, based on the x-ray diffraction data of

*annop.ektarawong@liu.se

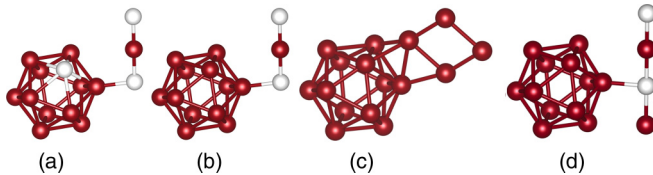


FIG. 1. Four structural motifs, used to model boron carbide in the present work, i.e., (a) $B_{11}C^p(\text{CBC})$, (b) $B_{12}(\text{CBC})$, (c) $B_{12}(B_4)$, and (d) $B_{12}(\text{CBCB})$. Instead of a linear chain, shown in (a), (b), and (d), the B_4 unit in (c) forms a rhombic chain. Red and white spheres represent B and C atoms, respectively.

boron-rich boron carbide [9]. Following the work of Shirai *et al.* [33], Rasim *et al.* [34,35] proposed extended structural models, dominated not only by $B_{11}C^p(\text{CBC})$, $B_{12}(\text{CBC})$, and $B_{12}(B_4)$, but also by $B_{12}(\text{CBCB})$ [Fig. 1(d)]. They found that the linear CBCB chain is capable of compensating for the electron deficiency in $B_{12}(\text{CBC})$ on the same level as the rhombic B_4 chains, and suggested both chain units are intrinsic defects for $B_{12}(\text{CBC})$. In addition, when the right fractions of $B_{11}C^p(\text{CBC})$, $B_{12}(\text{CBC})$, $B_{12}(B_4)$, and $B_{12}(\text{CBCB})$ are considered, the resulting configurations of boron carbide can be electron precise and low in energy, thus plausibly being an explanation to how the material retains its semiconducting character, as the carbon content varies within the single-phase region.

In this work, we perform first-principles calculations to investigate the phase stability, as well as electronic and elastic properties of boron carbide. The structural models of boron carbide are constructed through the combination of the four structural motifs, shown in Fig. 1. We find that the electron deficiency in $B_{12}(\text{CBC})$ can be compensated, if the motif is mixed with either $B_{12}(\text{CBCB})$ or $B_{12}(B_4)$ with a ratio of 2:1, which is in line with the findings, lately reported in Refs. [34,35]. Based on this rule, the composition of boron carbide is tuned from $B_{10.5}C$ to B_4C by varying the concentration of each structural motif, so that our constructed models of boron carbide are electron precise. We also aim not only to reveal the influence of configurational disorder of the four motifs on the phase stability and properties of the modeled boron carbides, which have so far not been considered, but also to demonstrate an implementation of the state-of-the-art cluster-expansion method [36] to search for ground-state configurations of boron carbide with compositions throughout the single-phase region, which are currently unknown, except B_4C .

Among several of our models, we identify three low-energy configurations, leading to a revolution of the B-C convex hull, i.e., $B_{11}C^p(\text{CBC})$, $[B_{12}(\text{CBC})]_{0.67}[B_{12}(\text{CBCB})]_{0.33}$, and $[B_{12}(\text{CBC})]_{0.67}[B_{12}(B_4)]_{0.33}$, corresponding to the compositions of B_4C , $B_{6.67}C$, and $B_{10.5}C$, respectively. As a consequence, $B_{12}(\text{CBC})$, previously proposed in the literature to be a stable configuration of boron carbide at the composition of $B_{6.5}C$, is no longer part of the convex hull. In addition, we observe large variation of electronic band gap, depending on the composition of boron carbide and the configuration of structural motifs, while the elastic moduli, derived from those identified low-energy configurations, are in fair agreement with the experiments. These findings highlight the importance of considering $B_{12}(\text{CBCB})$ and $B_{12}(B_4)$, together with

the previously proposed $B_{11}C^p(\text{CBC})$ and $B_{12}(\text{CBC})$, as the crucial ingredients for modeling boron carbide and support the idea proposed in Refs. [33–35]. Pushing further, we perform a ground-state search among the configurations of the structural units of $[B_{12}(\text{CBC})]_{0.67}[B_{12}(\text{CBCB})]_{0.33}$ and predict the ground-state configuration.

II. METHODOLOGY

A. Computational details

The first-principles total energies are calculated from the density functional theory (DFT), where the projector augmented wave (PAW) method [37] as implemented in the Vienna *ab initio* simulation package (VASP) [38,39] and the generalized gradient approximation (GGA) proposed by Perdew, Burke, and Ernzerhof (PBE96) [40] for the exchange-correlation functional are used. The plane-wave energy cutoff is set to 500 eV and the Monkhorst-Pack \mathbf{k} -point mesh [41] is chosen for the Brillouin zone integration. We also assure that the calculated total energies are converged within an accuracy of 1 meV/atom with respect to both the energy cutoff and the number of \mathbf{k} -point grids. During the total energy calculations, all internal atomic coordinates, volume, and cell shape are fully relaxed. The tetrahedron method for the Brillouin zone integrations, suggested by Blöchl [42], is used for electronic density of states calculations.

B. Structural models of boron carbide

In the present work, the structural models of boron carbide are constructed on the superatomic level, as implemented in the superatom-special quasirandom structure (SA-SQS) approach [20,21,32]. We note that, within the superatomic framework, a whole structural motif (icosahedron + chain) will be referred to as a superatom for the rest of this article. The models of boron carbide are constructed within various cell sizes, consisting of 15 up to 552 atoms, using the combination of the four superatomic species, proposed in the literature [33–35] (Fig. 1). Those are $B_{11}C^p(\text{CBC})$, $B_{12}(\text{CBC})$, $B_{12}(\text{CBCB})$, and $B_{12}(B_4)$. We note further that, apart from the four said structural motifs, other motifs, e.g., $B_{12}(\text{CCC})$, $B_{11}C(\text{BBC})$, $B_{12}(\text{BBC})$, etc., are not considered in the present work, as they are not energetically favorable from thermodynamic consideration, resulting in relatively high-energy configurations of boron carbide, and they are therefore unlikely to explain the discrepancies in the materials properties between theory and experiments, at least at low temperature [20,21,24]. Here, the composition of boron carbide varies between $B_{10.5}C$ and B_4C , depending on the concentration of each superatomic species. In order to achieve the electron-precise configurations, we compensate the electron deficiency in $B_{12}(\text{CBC})$ by employing the following rule:

$$x_{\text{CBC}} = 2(x_{\text{CBCB}} + x_{B_4}), \quad (1)$$

where x_{CBC} , x_{CBCB} , and x_{B_4} are the concentrations of $B_{12}(\text{CBC})$, $B_{12}(\text{CBCB})$, and $B_{12}(B_4)$, respectively. Detailed explanation of how such a rule is established will be further provided in Sec. III A.

In the present work, we consider 12 compositions. For all considered compositions, except $B_{6.5}C$ and B_4C , being represented by an individual superatom $B_{12}(CBC)$ and $B_{11}C^p(CBC)$, respectively, the superatoms are randomly distributed by using the special quasirandom structure (SQS) approach [43], such that their superatomic configurations are imitating the random alloy pattern. In addition, we also consider some selected ordered structures of superatoms, in particular at $B_{10.5}C$ and $B_{6.67}C$ compositions, represented by $[B_{12}(CBC)]_{0.67}[B_{12}(B_4)]_{0.33}$ and $[B_{12}(CBC)]_{0.67}[B_{12}(CBCB)]_{0.33}$, respectively, in order to assess the impact of superatomic configuration on the phase stability and properties of boron carbide at fixed compositions. The phase stability of all considered configurations of boron carbide is evaluated through the formation energy, calculated with respect to pure boron and carbon phases, i.e., α -boron and diamond, respectively,

$$\Delta E^{\text{form}}(B_m C_n) = \frac{E(B_m C_n) - [n \cdot E(B)] - [m \cdot E(C)]}{m + n}. \quad (2)$$

$\Delta E^{\text{form}}(B_m C_n)$ is the formation energy/atom of boron carbide $B_m C_n$ and $E(B_m C_n)$ is the total energy/formula unit of the compound. $E(B)$ and $E(C)$ are the total energies/atom of α -boron and diamond, respectively. We note that the influences of lattice vibrations, induced by temperature, are not studied in the present work and thus the phase stability as well as the intrinsic properties of boron carbide will, respectively, be evaluated and derived at 0 K. The information, such as concentrations for each superatomic species, formation energy with respect to the pure boron and carbon phases, and band gap, of the considered compositions and configurations of boron carbide is summarized in Table I.

C. Elastic properties calculations

To derive the elastic properties, strains ϵ with $\pm 1\%$ and $\pm 2\%$ distortions are applied to the supercells of boron carbide without volume conservation. We avoid residual stresses by relaxing the lattice parameters and the internal atomic coordinates, such that pressures are always less than 10^6 Pa. The elastic constant C_{ij} are then obtained from the second-order Taylor expansion of the total energy [44,45],

$$C_{ij} = \frac{1}{V_0} \left. \frac{\partial^2 E(\epsilon_1, \dots, \epsilon_6)}{\partial \epsilon_i \partial \epsilon_j} \right|_0, \quad (3)$$

in which Voigt's notation is used to describe the strain ϵ_i and the elastic tensor C_{ij} [46,47]. $E(\epsilon_1, \dots, \epsilon_6)$ is the total energy of the supercell, distorted by the correspondingly applied strains ϵ_i , while V_0 is the equilibrium volume of the undistorted supercell. It is worth noting that the inclusion of different superatomic species in modeling induces distortion, breaking the symmetry of boron carbide. Furthermore, the SQS approach in principle breaks the point-group symmetry. To deal with these issues, we employ the projection technique, suggested by Moakher *et al.* [48], to derive the rhombohedrally averaged elastic constants \bar{C}_{ij} , following the procedure described in our previous works on boron carbide [16,32]. Thus twelve independent elastic constants, i.e., C_{11} , C_{12} , C_{13} , C_{14} , C_{22} , C_{23} , C_{24} , C_{33} ,

C_{44} , C_{55} , C_{56} , and C_{66} , must be calculated to obtain the six averaged elastic constants, given by

$$\bar{C}_{11} = \frac{3}{8}(C_{11} + C_{22}) + \frac{1}{4}C_{12} + \frac{1}{2}C_{66}, \quad (4a)$$

$$\bar{C}_{12} = \frac{1}{8}(C_{11} + C_{22}) + \frac{3}{4}C_{12} - \frac{1}{2}C_{66}, \quad (4b)$$

$$\bar{C}_{13} = \frac{1}{2}(C_{13} + C_{23}), \quad (4c)$$

$$\bar{C}_{14} = \frac{1}{4}C_{14} - \frac{1}{4}C_{24} + \frac{1}{2}C_{56}, \quad (4d)$$

$$\bar{C}_{33} = C_{33}, \quad (4e)$$

$$\bar{C}_{44} = \frac{1}{2}C_{44} + C_{55}, \quad (4f)$$

$$\bar{C}_{66} = \frac{1}{2}(\bar{C}_{11} - \bar{C}_{12}). \quad (4g)$$

In the present work, we use the Voigt-Reuss-Hill (VRH) method [49] to determine isotropic polycrystalline elastic moduli of boron carbide.

III. RESULT AND DISCUSSION

A. Compensation of electron deficiency in $B_{12}(CBC)$

Based on the electron counting rule of Longuet-Higgins and Roberts [50] for interpreting the electronic structure and stability of icosahedral boron-rich clusters, 48 electrons/unit cell are required to complete the valence band of boron carbide and to result in a semiconducting state. This requirement is, however, only fulfilled for B_4C , represented by $B_{11}C^p(CBC)$. $B_{6.5}C$ represented by the idealized $B_{12}(CBC)$ is, on the other hand, electron-deficient due to the substitution of B for C^p atoms, resulting in one hole/unit cell. Ektarawong *et al.* [21] previously demonstrated that the electron-deficient state of $B_{12}(CBC)$ can be cured by thermally activated configurational disorder of B and C atoms. Such disorder, however, resulted in relatively high-energy configuration of boron carbide, which was predicted to be thermodynamically stable only at very high temperature.

Recently, another concept of compensating for the electron deficiency in $B_{12}(CBC)$ through the inclusion of either $B_{12}(B_4)$ or $B_{12}(CBCB)$ has been introduced, respectively, by Shirai *et al.* [33] and Rasim *et al.* [34,35]. In this section, we revisit such an issue in order to reveal a mechanism of both $B_{12}(B_4)$ and $B_{12}(CBCB)$ to compensate for the electron deficiency in $B_{12}(CBC)$.

To start with, we generate a $3 \times 2 \times 2$ supercell of the idealized $B_{12}(CBC)$ (180 atoms). Since $B_{12}(CBC)$ lacks one electron/unit cell, the generated supercell of $B_{12}(CBC)$ has 12 holes in the valence band, as shown in Fig. 2(a). We find that the exchange of a unit of $B_{12}(CBC)$ to either $B_{12}(CBCB)$ or $B_{12}(B_4)$ can compensate the electron deficiency for two additional units of $B_{12}(CBC)$, as can be seen from the number of holes in the valence band decreasing from 12 to 9 [Figs. 2(b) and 2(c)]. We note that a unit of $B_{12}(CBCB)$ or $B_{12}(B_4)$ can be considered as a dilute defect in a matrix of $B_{12}(CBC)$. Interestingly, both defective structures are stable with respect to the idealized $B_{12}(CBC)$ and pure boron phase, indicated by the negative formation energies (not shown). These findings are in line with the recent works [33–35], and will be served as a rule [Eq. (1)] for building up electron-precise superatomic configuration of boron carbide in the following sections.

TABLE I. Considered 12 compositions and 55 configurations of boron carbide. ΔE^{form} denotes the energy of formation, calculated with respect to α -boron and diamond. $\Delta\Delta E$ indicates the energy, relative to the convex hull (Fig. 3) at the same composition. E_g is the GGA-PBE96-calculated electronic band gap, while the numbers in the parentheses show the distance from the valence band edge to the midgap states, observed for $B_{4,313}C$ and $B_{4,306}C$.

Composition	at. % C	Supercell size (no. of atoms)	Percentages (%) of each superatomic species				ΔE^{form} (meV/atom)	$\Delta\Delta E$ (meV/atom)	E_g (eV)
			$B_{11}C^p(\text{CBC})$	$B_{12}(\text{CBC})$	$B_{12}(\text{CBCB})$	$B_{12}(B_4)$			
$B_{10,5}C$	8.695	$3 \times 2 \times 2$ (184)		66.67		33.33	-69.701	6.473	0.990
		$3 \times 2 \times 2$ (184)		66.67		33.33	-70.550	5.624	1.617
		$3 \times 2 \times 2$ (184)		66.67		33.33	-75.053	1.121	1.671
		$3 \times 2 \times 2$ (184)		66.67		33.33	-59.157	17.017	metal
		$3 \times 2 \times 2$ (184)		66.67		33.33	-72.438	3.736	0.994
		$3 \times 2 \times 2$ (184)		66.67		33.33	-73.373	28.009	1.375
		$3 \times 2 \times 2$ (184)		66.67		33.33	-75.338	0.836	1.310
		$3 \times 3 \times 2$ (276)		66.67		33.33	-76.174	0	1.345
		$3 \times 3 \times 2$ (276)		66.67		33.33	-64.865	11.309	1.184
		$3 \times 3 \times 2$ (276)		66.67		33.33	-73.328	2.846	0.890
		$3 \times 3 \times 2$ (276)		66.67		33.33	-73.416	2.758	1.568
		$3 \times 3 \times 2$ (276)		66.67		33.33	-70.913	5.261	1.116
		$3 \times 3 \times 2$ (276)		66.67		33.33	-72.460	3.714	1.210
		$3 \times 3 \times 2$ (276)		66.67		33.33	-72.216	3.958	1.248
		$3 \times 3 \times 2$ (276)		66.67		33.33	-74.828	1.346	1.008
		$3 \times 3 \times 3$ (414)		66.67		33.33	-46.813	29.361	0.653
		$3 \times 3 \times 3$ (414)		66.67		33.33	-71.844	4.330	0.952
		$3 \times 3 \times 3$ (414)		66.67		33.33	-71.125	5.049	1.089
		$4 \times 3 \times 3$ (552)		66.67		33.33	-69.202	6.972	0.994
		$4 \times 3 \times 3$ (552)		66.67		33.33	-72.702	3.472	1.185
$4 \times 3 \times 3$ (552)		66.67		33.33	-74.245	1.929	1.606		
$B_{8,857}C$	10.145	$3 \times 3 \times 2$ (276)		66.67	11.11	22.22	-81.050	2.589	1.406
$B_{6,956}C$	12.568	$4 \times 3 \times 3$ (549)	25	50	8.33	16.67	-84.412	11.709	0.937
$B_{6,67}C$	13.043	$3 \times 2 \times 2$ (184)		66.67		33.33	-86.396	12.172	0.131
		$3 \times 2 \times 2$ (184)		66.67		33.33	-94.267	4.301	0.969
		$3 \times 2 \times 2$ (184)		66.67		33.33	-95.110	3.458	1.445
		$3 \times 2 \times 2$ (184)		66.67		33.33	-77.333	21.235	metal
		$3 \times 2 \times 2$ (184)		66.67		33.33	-98.260	0.308	1.550
		$3 \times 2 \times 2$ (184)		66.67		33.33	-92.563	6.005	0.980
		$3 \times 2 \times 2$ (184)		66.67		33.33	-96.499	2.069	1.119
		$3 \times 3 \times 2$ (276)		66.67		33.33	-98.568	0	1.674
		$3 \times 3 \times 2$ (276)		66.67		33.33	-94.514	4.054	1.342
		$3 \times 3 \times 2$ (276)		66.67		33.33	-85.129	13.439	0.390
		$3 \times 3 \times 2$ (276)		66.67		33.33	-95.228	3.339	1.370
		$3 \times 3 \times 2$ (276)		66.67		33.33	-97.744	0.824	1.405
		$3 \times 3 \times 2$ (276)		66.67		33.33	-88.863	9.705	0.328
		$3 \times 3 \times 2$ (276)		66.67		33.33	-93.211	5.358	0.879
		$3 \times 3 \times 2$ (276)		66.67		33.33	-94.230	4.338	1.018
		$3 \times 3 \times 3$ (414)		66.67		33.33	-83.353	15.215	1.215
		$3 \times 3 \times 3$ (414)		66.67		33.33	-91.852	6.716	0.918
		$3 \times 3 \times 3$ (414)		66.67		33.33	-93.928	4.639	1.148
		$4 \times 3 \times 3$ (552)		66.67		33.33	-89.339	9.229	0.539
		$4 \times 3 \times 3$ (552)		66.67		33.33	-92.711	5.856	0.667
$4 \times 3 \times 3$ (552)		66.67		33.33	-92.941	5.627	1.010		
$B_{6,611}C$	13.138	$4 \times 3 \times 3$ (548)	33.33	44.44	5.56	16.67	-83.750	15.224	1.356
$B_{6,6}C$	13.158	$5 \times 3 \times 2$ (456)	40	40		20	-89.380	9.676	1.137
$B_{6,5}C$	13.333	$1 \times 1 \times 1$ (15)		100			-90.142	9.662	metal
$B_{6,21}C$	13.868	$4 \times 3 \times 3$ (548)	33.34	44.44	11.11	11.11	-88.136	13.952	0.667
$B_{6,125}C$	14.035	$5 \times 3 \times 2$ (456)	40	40	6.67	13.33	-89.962	12.836	0.656
$B_{4,313}C$	18.819	$3 \times 3 \times 2$ (271)	94.44			5.56	-112.667	10.541	2.392
		$3 \times 3 \times 2$ (271)	83.33	11.11	5.56		-114.917	8.291	2.169 (1.167)

TABLE I. (Continued.)

Composition	at. % C	Supercell size (no. of atoms)	Percentages (%) of each superatomic species				ΔE^{form} (meV/atom)	$\Delta\Delta E$ (meV/atom)	E_g (eV)
			$B_{11}C^p(\text{CBC})$	$B_{12}(\text{CBC})$	$B_{12}(\text{CBCB})$	$B_{12}(\text{B}_4)$			
$B_{4.306}C$	18.847	$5 \times 3 \times 2$ (451)	90	6.67		3.33	-118.524	4.802	1.979 (0.987)
		$5 \times 3 \times 2$ (451)	90	6.67		3.33	-120.944	2.383	2.967 (1.916)
		$5 \times 3 \times 2$ (451)	90	6.67		3.33	-121.452	1.875	2.975 (1.755)
B_4C	20	$1 \times 1 \times 1$ (15)	100				-128.246	0	3

Although $B_{12}(\text{CBCB})$ and $B_{12}(\text{B}_4)$ units are capable of compensating the electron deficiency in $B_{12}(\text{CBC})$ at the same level, their mechanisms are somewhat different. By further inspecting the number of electronic states of the valence band, we find that replacing $B_{12}(\text{CBC})$ by $B_{12}(\text{CBCB})$ gives rise to four midgap states [see Fig. 2(b)], but the number of electronic states of the valence band remains unchanged. In this particular case, the number of holes reduces from 12 to 9 through three additional valence electrons from the extra B atom in the chain. On the other hand, replacing $B_{12}(\text{CBC})$ by $B_{12}(\text{B}_4)$ does reduce the total number of electronic states of the valence band by 2. Those states might be split off from the valence band and become part of the midgap states [see Fig. 2(c)]. Considering this together with the fact that the B_4 chain possesses a valence electron more than the CBC chain, there remain in total nine holes in the valence band.

B. Revolution of the B-C convex hull

We note that, to achieve electron-precise superatomic configurations, we restrict ourselves to the four superatomic species, shown in Fig. 1, as well as the rule of compensating the electron deficiency for $B_{12}(\text{CBC})$ [Eq. (1)], established from the findings in the previous subsection. In this particular case, we consider in total 55 configurations of boron carbide, and its composition ranges from

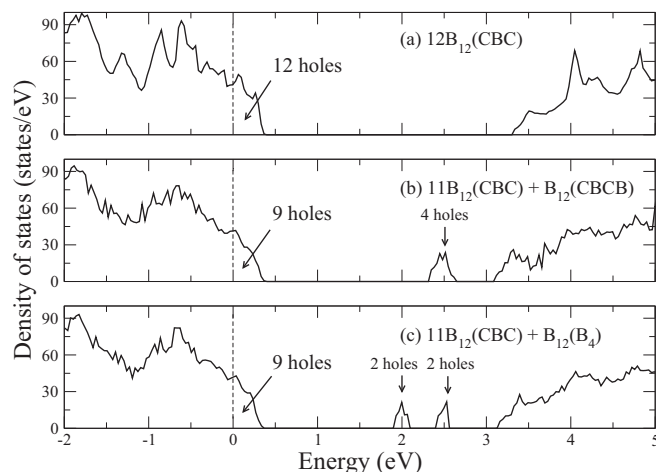


FIG. 2. Density of states of (a) $12B_{12}(\text{CBC})$, (b) $11B_{12}(\text{CBC}) + B_{12}(\text{CBCB})$, and (c) $11B_{12}(\text{CBC}) + B_{12}(\text{B}_4)$. The highest occupied state is located at 0 eV and indicated by the dashed line.

$B_{10.5}C$ to B_4C , in particular at $B_{10.5}C$ and $B_{6.67}C$ compositions, represented by $[B_{12}(\text{CBC})]_{0.67}[B_{12}(\text{B}_4)]_{0.33}$ and $[B_{12}(\text{CBC})]_{0.67}[B_{12}(\text{CBCB})]_{0.33}$, respectively. Table I lists the information, e.g., concentrations for each superatomic species, formation energy with respect to the pure boron and carbon phases, and electronic band gap, of all 55 configurations of boron carbide. Figure 3 illustrates the formation energies ΔE^{form} of the 55 configurations of boron carbide, calculated with respect to pure boron and carbon phases, i.e., α -boron and diamond, respectively.

As shown in Fig. 3, several of our superatomic configurations are relatively stable with respect to the idealized $B_{12}(\text{CBC})$ (open black circle), previously proposed to be part of the B-C convex hull, together with $B_{11}C^p(\text{CBC})$ (dashed lines) [20–27]. Among those, we identify three low-energy configurations (filled solid circles), resulting in a revolution of the convex hull (thick solid lines). Those are $B_{11}C^p(\text{CBC})$, $[B_{12}(\text{CBC})]_{0.67}[B_{12}(\text{CBCB})]_{0.33}$, and $[B_{12}(\text{CBC})]_{0.67}[B_{12}(\text{B}_4)]_{0.33}$, corresponding to compositions of B_4C , $B_{6.67}C$, and $B_{10.5}C$, respectively. As a result, $B_{12}(\text{CBC})$ at $B_{6.5}C$ composition is no longer a stable configuration, as it is clearly above the convex hull. Our obtained results are in

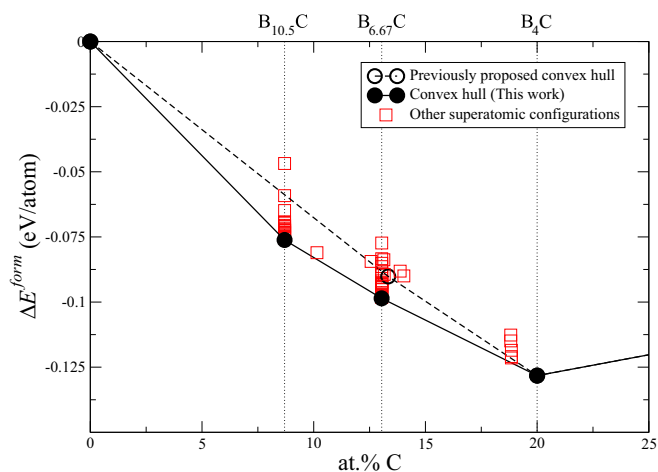


FIG. 3. Formation energy ΔE^{form} of boron carbide, calculated with respect to α boron and diamond. A set of thick solid lines, connecting filled black circles at $B_{10.5}C$, $B_{6.67}C$, and B_4C , indicates the B-C convex hull, derived from all of the configurations, listed in Table I. A set of dashed lines, on the other hand, indicates the previously proposed convex hull, consisting of $B_{6.5}C$, given by $B_{12}(\text{CBC})$ (open black circle) and B_4C .

line with the findings, recently reported in Refs. [34,35], and also confirm the theoretical prediction, suggested by Shirai *et al.* [33], that $B_{12}(\text{CBC})$ is not the lowest energy configuration of $B_{6.5}\text{C}$.

We emphasize that, although the two configurations at $B_{6.67}\text{C}$ and $B_{10.5}\text{C}$, being part of our sketched B-C convex hull [Fig. 3], possess the lowest energy, as compared to the other configurations considered at the same composition, there is no guarantee that such configurations are really their global minimum in energy, i.e., ground state, at the corresponding compositions. It is worth noting that there are indeed a number of ways to define a superatomic formula at one particular composition. For example, rather than $[B_{12}(\text{CBC})]_{0.67}[B_{12}(\text{CBCB})]_{0.33}$, the superatomic formula of $B_{6.67}\text{C}$ can be given by

$$[B_{11}\text{C}^p(\text{CBC})]_{23/59}[B_{12}(\text{CBC})]_{24/59}[B_{12}(\text{B}_4)]_{12/59}.$$

In principle, at a given composition of boron carbide, one needs to consider all possible superatomic formulas and configurations, before a final conclusion concerning the ground state at that composition can be drawn.

However, it should also be noted that determining the ground-state configurations of boron carbide at any given carbon content and configurational phase transitions at elevated temperatures is a huge challenge to the alloy theoreticians even at the superatomic level due to a variety of superatomic species of boron carbide, leading to the problems typical of multicomponent alloys. In the present work, an attempt to search for the ground-state configuration of $[B_{12}(\text{CBC})]_{0.67}[B_{12}(\text{CBCB})]_{0.33}$ has been made, and will be discussed in Sec. III D.

Concerning the phase stability of $B_{\sim 4.3}\text{C}$, having been claimed in experiment to be the upper limit of the carbon content for boron carbide, we have demonstrated in Table I that the structural models of $B_{4.3}\text{C}$, that are composed of $B_{12}(\text{B}_4)$, $B_{12}(\text{CBC})$, and $B_{11}\text{C}^p(\text{CBC})$ and are electron precise, exhibit relatively low-energy configurations. Their formation energies were found to be less than 5 meV/atom above the revised B-C convex hull at 0 K; see Table I and also Fig. 3. One would thus expect that $B_{4.3}\text{C}$ is thermodynamically favored over $B_4\text{C}$ at elevated temperature due to the mixing entropy. This might also be an explanation of why synthesizing boron carbide with the stoichiometric composition of $B_4\text{C}$ (20 at. % C) at high temperature in general results in a mixture of boron carbide with the carbon content slightly lower than 20 at. % and free graphitelike carbon [7,51,52].

C. Electronic and elastic properties of boron carbide

Besides the phase stability, as discussed in the previous section, our calculations also reveal dependencies of composition and configuration on the electronic properties of boron carbide. We observe that, for those electron precise configurations, the electronic band gap largely varies between 0.1 and 3.0 eV, as can be seen from Table I. For instance, the band gap of the identified low-energy ordered configuration of $B_{6.67}\text{C}$ ($B_{10.5}\text{C}$) is 1.67 (1.35) eV. The band gap, however, shrinks to 0.54 (0.99) eV, when its superatomic configuration is that of a random alloy, illustrated in Fig. 4. On the other hand, the indirect band gap of boron carbide has been experimentally reported to fall into the range between 0.48 and 2.09 eV, depending on its stoichiometry [55–58]. By taking into account

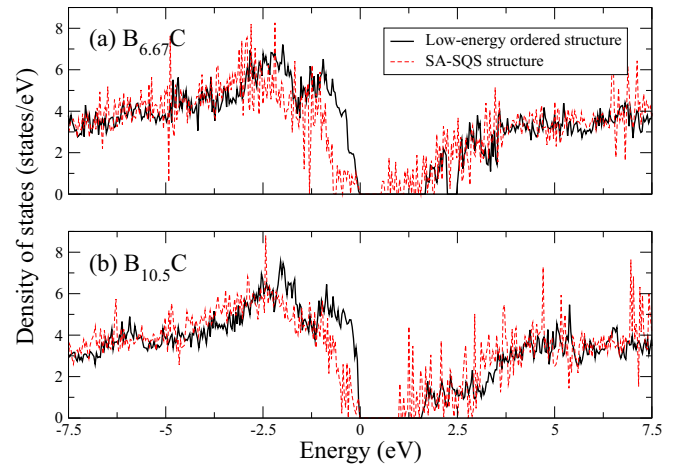


FIG. 4. GGA-PBE96-calculated electronic density of states of (a) $B_{6.67}\text{C}$ or $[B_{12}(\text{CBC})]_{0.67}[B_{12}(\text{CBCB})]_{0.33}$ and (b) $B_{10.5}\text{C}$ or $[B_{12}(\text{CBC})]_{0.67}[B_{12}(\text{B}_4)]_{0.33}$. The highest occupied state is located at 0 eV. The black solid and red dashed lines denote, respectively, the density of states of the lowest-energy configurations, identified in Sec. III B, and of that imitating the random alloy pattern, respectively.

also the fact that local and semilocal functionals, such as LDA and GGA, typically underestimate the band gap of semiconductors and insulators, the structural models of boron carbide, composed either of $B_{12}(\text{CBCB})$ or of $B_{12}(\text{B}_4)$ to compensate for the electron deficiency in $B_{12}(\text{CBC})$, yield a good description of electronic band gap, which is in line with experiments and likely to be an explanation to how boron carbide retains its semiconducting state, as the carbon content varies within the single-phase region.

Apart from the idealized $B_{12}(\text{CBC})$, we observed two superatomic configurations, one at $B_{6.67}\text{C}$ and the other at $B_{10.5}\text{C}$, behaving as a metal. We note that these configurations have been built upon the rule [Eq. (1)], established from the findings in Sec. III A, and were supposed to be semiconductors. The source of their metallic character may be attributed to the overlapping between the fully occupied valence band and unoccupied midgap states, thus resulting in an unfavorably high-energy configuration. The influence of superatomic arrangement on electronic properties of boron carbide has, however, remained ambiguous, thus deserving further investigation. We, moreover, consider the elastic properties of boron carbide by focusing on the three identified low-energy ordered configurations at $B_{10.5}\text{C}$, $B_{6.67}\text{C}$, and $B_4\text{C}$ compositions. In the present work, we calculate the elastic constants and moduli of $[B_{12}(\text{CBC})]_{0.67}[B_{12}(\text{CBCB})]_{0.33}$ and $[B_{12}(\text{CBC})]_{0.67}[B_{12}(\text{B}_4)]_{0.33}$, while those of $B_{11}\text{C}^p(\text{CBC})$ are taken from our previous work of boron carbide [32], also calculated using the approach described in Sec. II C. Note that the reliability of our approach, used to calculate the elastic properties of boron carbide, has been confirmed and discussed in Ref. [32]. The elastic moduli of boron carbide, calculated in the present and our previous works, as well as the corresponding experimental data, available in the literature, are given in Table II, and Fig. 5 illustrates a comparison between the experimentally measured and calculated Young's modulus of boron carbide at different compositions. For comparison

TABLE II. Calculated averaged elastic constants \bar{C}_{ij} , bulk modulus B_H , shear modulus G_H , and Young's modulus E_H of boron carbide and α -boron, obtained from the Voigt-Reuss-Hill (VRH) approach. Experimental values of elastic moduli, available in the literature, are given in parentheses for a comparison purpose. The unit for elastic constants and moduli are GPa.

Composition	Configuration	\bar{C}_{11}	\bar{C}_{12}	\bar{C}_{13}	\bar{C}_{14}	\bar{C}_{33}	\bar{C}_{44}	B_H	G_H	E_H	Ref.
B ₄ C	B ₁₁ C ^p (CBC)	559	123	68	24	524	169	239 (247) (235)	200 (200) (197)	469 (472) (462)	[32] ^a [53] ^b [54] ^c
B _{4.5} C						(237)		(197)	(197)	(463)	[53] ^b
B _{5.6} C						(236)		(197)	(197)	(462)	[53] ^b
B _{6.5} C	B ₁₂ (CBC)	516	118	74	7	451	106	222	156	379	[32] ^a
	[B ₁₂ (CBC)] _{0.5} [B ₁₁ C ^e (BBC)] _{0.5}	523	122	69	21	471	170	225	190	445	[32] ^a
						(231)		(189)	(189)	(446)	[53] ^b
B _{6.67} C	[B ₁₂ (CBC)] _{0.67} [B ₁₂ (CBCB)] _{0.33}	504	125	69	26	547	146	231	177	423	This work
B _{7.7} C						(178)		(150)	(150)	(352)	[53] ^b
B ₉ C						(183)		(150)	(150)	(319)	[53] ^b
						(130)		(132)	(132)	(348)	[53] ^b
B _{10.5} C	[B ₁₂ (CBC)] _{0.67} [B ₁₂ (B ₄)] _{0.33}	506	104	73	6	492	170	222	195	452	This work
B	B ₁₂ (α -boron)	453	110	40	26	606	207	210	200	457	This work

^aReference [32]: Ektarawong *et al.* (GGA).

^bReference [53]: Gieske *et al.* (Expt.).

^cReference [54]: Manghnani *et al.* (Expt.).

purposes, the elastic constants and moduli of α -boron or B₁₂, derived in this work, are also provided in Table II, and they are in good agreement with the previous calculations, performed by He and Zhong [59].

As can be seen from Table II and Fig. 5, the elastic moduli of B₄C, given by B₁₁C^p(CBC), are in excellent agreement with the experiments [53,54]. On the other hand, the Young's and shear moduli of B_{6.5}C, represented by the idealized B₁₂(CBC), are to a large extent underestimated, as compared to the experiment [53]. We, however, find that a close agreement with the experiment at around B_{6.5}C composition

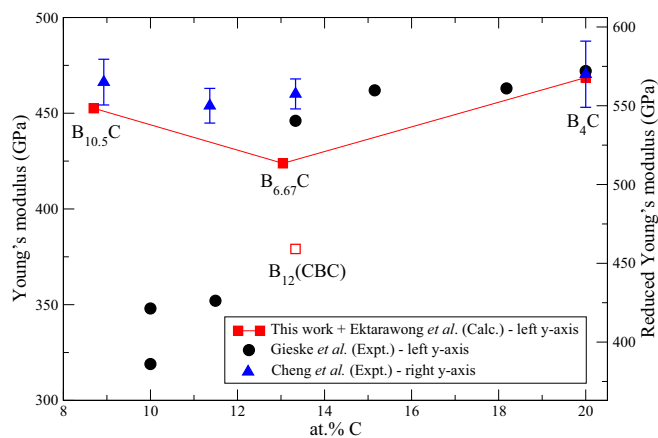


FIG. 5. Young's modulus of boron carbide, plotted as a function of carbon content (left y axis). The experimentally measured Young's modulus (filled black circles) are taken from the work of Gieske *et al.* [53], while the theoretical values (filled and open red squares) are obtained from the calculations in the present and our previous work [32]. Filled blue triangles represent the experimental reduced Young's modulus of boron carbide at different carbon content (right y axis), reported by Cheng *et al.* [60].

can be achieved, when the electron deficiency in B₁₂(CBC) is compensated by B₁₂(CBCB), as can be seen from the elastic moduli of B_{6.67}C or [B₁₂(CBC)]_{0.67}[B₁₂(CBCB)]_{0.33}, calculated in the present work. Such an increase in elastic moduli was previously observed in [B₁₂(CBC)]_{0.5}[B₁₁C^e(BBC)]_{0.5}, in which B₁₁C^e(BBC) compensates for the electron deficiency in B₁₂(CBC) [32]. The superscript *e* denotes the equatorial sublattice. We thus attribute this to the band-filling effects, resulting in a semiconducting state of boron carbide.

Owing to the band-filling effects, the elastic moduli of B_{10.5}C or [B₁₂(CBC)]_{0.67}[B₁₂(B₄)]_{0.33} are comparable to those of B_{6.67}C and B₄C. Apparently, the calculated results of B_{10.5}C contradict the experimental elastic moduli reported by Gieske *et al.* [53] for B_{7.7}C and B₉C (see Table II and Fig. 5). They suggested that, on the boron-rich side (at. % C < 13.33), boron carbide becomes substantially compressible because of B₁₂, replacing B₁₁C, in this composition range. However, our results demonstrate that such a statement may not be true, as all of the icosahedra, composing B_{10.5}C, are B₁₂. Cheng *et al.* [60] have, recently, reported the experimentally measured reduced Young's modulus of boron carbide at different carbon content, showing that the quantity barely changes with the carbon content (see Fig. 5), qualitatively in line with our calculations, while the drastic softening of elastic moduli, observed for B_{7.7}C and B₉C in Ref. [53], may be attributed to porosity of the as-synthesized boron carbide samples at those compositions.

We have demonstrated that both the electronic and elastic properties of boron carbides of which the electron deficiency in B₁₂(CBC) are fully compensated either by B₁₂(CBCB) or by B₁₂(B₄) are in agreement with the experimental observations. Considering this together with the findings on the phase stability of boron carbide in the previous section, we highlight the importance of considering B₁₂(CBCB) and B₁₂(B₄), as well as the previously proposed B₁₁C^p(CBC) and B₁₂(CBC), as the principal structural building blocks for modeling boron

TABLE III. 23 superatomic configurations of $[\text{B}_{12}(\text{CBC})]_{0.67}[\text{B}_{12}(\text{CBCB})]_{0.33}$ and their Warren-Cowley short-range-order (SRO) parameters (α_i) for the first eight coordination shells ($i = 1-8$). $E^{\gamma\text{-DFT}}$ and $E^{\gamma\text{-CE}}$ stand for the total energies per superatom (eV/s.a.), calculated from DFT and from Eq. (6), using the fitting parameters, given by Eq. (7), respectively.

Conf. γ	Supercell size (no. of atoms)	Warren-Cowley short-range-order (SRO) parameters (α_i)								$E^{\gamma\text{-DFT}}$	$E^{\gamma\text{-CE}}$
		α_1	α_2	α_3	α_4	α_5	α_6	α_7	α_8		
1	$3 \times 2 \times 2$ (184)	0	0	-1/8	0	-1/8	-1/8	1/2	0	-108.546	-108.586
2	$3 \times 2 \times 2$ (184)	-1/2	1/2	-1/2	1/2	-1/4	0	1/2	0	-108.666	-108.651
3	$3 \times 2 \times 2$ (184)	-3/8	1/4	-1/2	1/4	-1/8	0	5/8	1/4	-108.679	-108.684
4	$3 \times 2 \times 2$ (184)	1/2	0	-1/2	0	0	-1/2	1/2	0	-108.407	-108.396
5	$3 \times 2 \times 2$ (184)	-1/4	-1/4	5/8	-1/4	-1/4	-1/8	3/4	1/2	-108.727	-108.726
6	$3 \times 2 \times 2$ (184)	1/8	-1/4	-1/2	-1/4	1/8	-1/4	7/8	3/4	-108.640	-108.642
7	$3 \times 2 \times 2$ (184)	-1/4	-1/8	1/4	-1/8	-3/16	1/8	1/2	0	-108.700	-108.712
8	$3 \times 3 \times 2$ (276)	-1/6	-1/3	1/3	-1/6	-1/12	1/3	1/3	-1/6	-108.732	-108.734
9	$3 \times 3 \times 2$ (276)	-1/2	1/2	-1/4	0	-1/4	0	0	0	-108.670	-108.659
10	$3 \times 3 \times 2$ (276)	0	0	1/2	-1/2	-1/2	-1/2	0	0	-108.526	-108.551
11	$3 \times 3 \times 2$ (276)	0	-1/4	-1/2	0	1/4	0	1/2	1/4	-108.681	-108.691
12	$3 \times 3 \times 2$ (276)	-1/3	0	1/4	0	-1/12	-1/6	1/6	-1/6	-108.719	-108.715
13	$3 \times 3 \times 2$ (276)	-1/12	1/12	-1/6	1/6	1/24	-1/3	1/4	-1/6	-108.583	-108.604
14	$3 \times 3 \times 2$ (276)	-1/6	0	1/6	0	-1/12	-1/3	1/6	-1/6	-108.650	-108.646
15	$3 \times 3 \times 2$ (276)	0	-1/6	1/3	-1/3	-1/4	-1/6	1/3	0	-108.665	-108.616
16	$3 \times 3 \times 3$ (414)	-1/2	1	-1/2	-1/2	-1/2	1	-1/2	1	-108.499	-108.504
17	$3 \times 3 \times 3$ (414)	-1/9	0	-1/9	2/9	2/9	-1/2	-1/9	0	-108.629	-108.634
18	$3 \times 3 \times 3$ (414)	-1/9	-1/6	1/18	-1/9	-1/9	1/2	-1/9	-1/6	-108.661	-108.661
19	$4 \times 3 \times 3$ (552)	0	0	-1/24	0	0	0	0	0	-108.591	-108.577
20	$4 \times 3 \times 3$ (552)	0	-1/8	-10/24	0	5/24	-5/24	5/24	1/3	-108.642	-108.643
21	$4 \times 3 \times 3$ (552)	-1/12	-1/6	-1/2	-1/6	3/16	-1/4	10/24	13/24	-108.646	-108.632
22 ^a	$18 \times 18 \times 18$ (89 424)	-1/2	0	0	1/2	10/24	-1/3	-1/3	-1/6		-108.794
23	$4 \times 3 \times 3$ (552)	-1/2	0	0	1/2	3/8	-1/4	-1/4	-1/4	-108.756	-108.795

^aGround state, predicted by Monte Carlo simulations.

carbide, whose frequency of occurrence varies with the global composition within the single-phase region of boron carbide. This is distinctly in line with the recent work, done by Shirai *et al.* [33] and Rasim *et al.* [34,35].

D. Search for the ground-state configuration of $[\text{B}_{12}(\text{CBC})]_{0.67}[\text{B}_{12}(\text{CBCB})]_{0.33}$

In Sec. III B, we have pointed out a challenge to investigating the influence of configuration on phase stability and properties of boron carbide owing to its structural complexity and large solubility of carbon, resulting in a large variety of structural building blocks and the order among them. Despite such a challenge, we endeavor in the present section to determine the ground state of $[\text{B}_{12}(\text{CBC})]_{0.67}[\text{B}_{12}(\text{CBCB})]_{0.33}$. To do so, we employ the Connolly-Williams cluster expansion (CE) method [36] on the level of $\text{B}_{12}(\text{CBC})$ and $\text{B}_{12}(\text{CBCB})$ superatoms in order to derive the so-called effective cluster interactions (ECIs),

$$E^\gamma = E' + \sum_f V_f^{(n)} \xi_f^{(n)-\gamma}. \quad (5)$$

E^γ is the total energy of $[\text{B}_{12}(\text{CBC})]_{0.67}[\text{B}_{12}(\text{CBCB})]_{0.33}$ for a given configuration γ . $\xi_f^{(n)-\gamma}$ and $V_f^{(n)}$ are the n -site correlation function of a specific figure f , defined for the configuration γ , and the n -site ECI of a specific figure f , respectively. The term E' is the total energy of $[\text{B}_{12}(\text{CBC})]_{0.67}[\text{B}_{12}(\text{CBCB})]_{0.33}$, imitating the configuration of a random alloy stable in the limit of $T \rightarrow \infty$, where $\xi_f^{(n)} = 0$ for any n and f .

Even though the expansion, expressed in Eq. (5), is analytically exact in the limit of inclusion of all possible figures, it must be truncated for practical purposes. For this particular case, we only consider two-site figures up to the eighth coordination shell. Thus $\xi_f^{(n)-\gamma}$ can be defined as the Warren-Cowley short-range-order (SRO) parameter, α_i , representing the two-site correlation function for the i th coordination shell, and $V_f^{(n)}$ reduces to $V_i^{(2)}$, which is the effective pair interaction of the i th coordination shell. Equation (5) can then be rewritten as

$$E^\gamma = E' + \sum_{i=1}^8 V_i^{(2)} n_i \alpha_i^\gamma. \quad (6)$$

n_i is the number of neighbors in the i th shell. In the case of boron carbide, $n_i = 6$ for $i = 1-4$ and $6-8$, while $n_5 = 12$. To solve for the unknown quantities in Eq. (6), i.e., E' and $V_i^{(2)}$, we model a set of different configurations of γ of $[\text{B}_{12}(\text{CBC})]_{0.67}[\text{B}_{12}(\text{CBCB})]_{0.33}$ with each γ defined by a particular set of α_i^γ , and then determine E^γ , using DFT calculations. E' and $V_i^{(2)}$ can then be obtained by performing a least-squares fit to the set of Eq. (6). Table III lists the SRO parameters (α_i ; $i = 1-8$) for 21 superatomic configurations of $[\text{B}_{12}(\text{CBC})]_{0.67}[\text{B}_{12}(\text{CBCB})]_{0.33}$, labeled by configuration $\gamma = 1-21$, and their total energies per superatom (s.a.), $E^{\gamma\text{-DFT}}$, obtained from DFT calculations. Through the input from the 21 configurations, the fitting parameters (Hamiltonian), i.e., E'

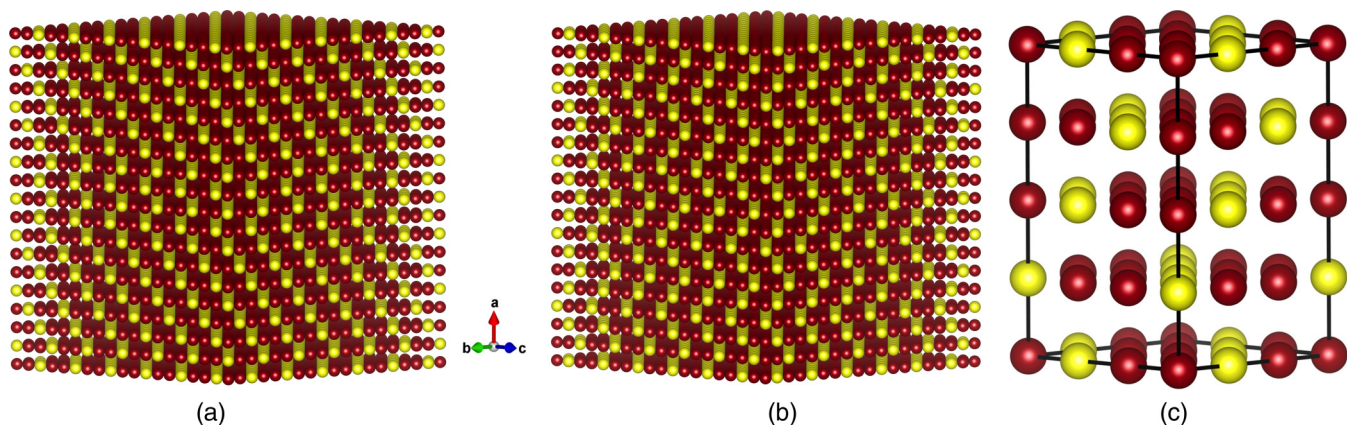


FIG. 6. (a) Superatomic ground-state configuration of $[\text{B}_{12}(\text{CBC})]_{0.67}[\text{B}_{12}(\text{CBCB})]_{0.33}$, predicted from Monte Carlo simulations (the 22nd configuration, listed in Table III), (b) superatomic configuration of $[\text{B}_{12}(\text{CBC})]_{0.67}[\text{B}_{12}(\text{CBCB})]_{0.33}$, imitating the SRO parameters of (a) up to the fourth coordination shell (the 23rd configuration, listed in Table III), and (c) proposed primitive unit cells of the ground state of $[\text{B}_{12}(\text{CBC})]_{0.67}[\text{B}_{12}(\text{CBCB})]_{0.33}$, derived from (b) and represented by a supercell composed of $4 \times 3 \times 3$ rhombohedral primitive unit cells of boron carbide. The red and yellow spheres represent $\text{B}_{12}(\text{CBC})$ and $\text{B}_{12}(\text{CBCB})$ superatoms, respectively.

and $V_i^{(2)}$ ($i = 1-8$) in eV/s.a., are given as follows:

$$\begin{pmatrix} E' \\ V_1^{(2)} \\ V_2^{(2)} \\ V_3^{(2)} \\ V_4^{(2)} \\ V_5^{(2)} \\ V_6^{(2)} \\ V_7^{(2)} \\ V_8^{(2)} \end{pmatrix} = \begin{pmatrix} -108.5746 \\ 0.0742 \\ 0.0443 \\ 0.0085 \\ 0.0111 \\ -0.0062 \\ 0.0018 \\ -0.0042 \\ 0.0043 \end{pmatrix}. \quad (7)$$

The total energy of $[\text{B}_{12}(\text{CBC})]_{0.67}[\text{B}_{12}(\text{CBCB})]_{0.33}$, calculated from the fitting parameters ($E^{\gamma\text{-CE}}$), are also given in Table III. We find that our Hamiltonian fits the 21 input configurations with a root-mean-square error of 17.47 meV/s.a., confirming its reliability of predicting the total energy of $[\text{B}_{12}(\text{CBC})]_{0.67}[\text{B}_{12}(\text{CBCB})]_{0.33}$.

We then utilize the obtained Hamiltonian in canonical Monte Carlo (MC) simulations in order to search for a candidate, representing the ground-state configuration of $[\text{B}_{12}(\text{CBC})]_{0.67}[\text{B}_{12}(\text{CBCB})]_{0.33}$. In this case, we use simulation boxes of $18 \times 18 \times 18$ rhombohedral unit cell (89 424 atoms), and the MC simulations are performed by using Metropolis *et al.* [61] algorithm. During the simulations, the material is cooled from 4000 to 0 K, using simulated annealing with the temperature steps 100 K and 50 K for $T > 2000$ K and $T < 2000$ K, respectively. At each temperature, the simulations include 20 000 Monte Carlo steps for equilibrating the system and then 10000 more steps for obtaining the proper averages of the total energies and SRO parameters. The total energy $E^{\gamma\text{-CE}}$ as well as the SRO parameters of $[\text{B}_{12}(\text{CBC})]_{0.67}[\text{B}_{12}(\text{CBCB})]_{0.33}$, resulting from the MC simulations at $T = 0$ K, are listed in Table III and denoted by the 22nd configuration.

As visualized in Fig. 6(a), the MC predicted ground state of $[\text{B}_{12}(\text{CBC})]_{0.67}[\text{B}_{12}(\text{CBCB})]_{0.33}$ can be viewed from the superatomic perspective as a stacking sequence of

$[\text{B}_{12}(\text{CBC})]_{0.67}[\text{B}_{12}(\text{CBCB})]_{0.33}$ layers along the $[100]_r$ direction, by which each layer assembles a repeat pattern of two columns of $\text{B}_{12}(\text{CBC})$ and a column of $\text{B}_{12}(\text{CBCB})$ along the $[011]_r$. In order to verify our prediction, the total energy of the MC predicted ground state must have been calculated from DFT, and compared to the other configurations. Direct DFT calculations of such a large supercell (89 424 atoms) is, however, not feasible. As a consequence, we estimate the total energy $E^{\gamma\text{-DFT}}$ of the MC ground state by constructing the 23rd configuration of $[\text{B}_{12}(\text{CBC})]_{0.67}[\text{B}_{12}(\text{CBCB})]_{0.33}$ within a much smaller $4 \times 3 \times 3$ supercell (552 atoms), whose SRO parameters imitate those of the MC predicted ground state up to the fourth shell. As can be seen from Fig. 6(b), the 23rd configuration exhibits exactly identical in-plane superatomic configuration to that of the MC predicted ground state, while their stacking features are only slightly different. In addition, the total energies of the two configurations predicted by the Hamiltonian are very similar (see Table III), implying that the 23rd configuration can be reasonably used for estimating the phase stability of the MC predicted ground state. Interestingly, the DFT energy $E^{\gamma\text{-DFT}}$ of the 23rd configuration is lowest, as compared to the other 21 configurations, and it results in the formation energy ΔE^{form} of -0.1 eV/atom with respect to α -boron and diamond, which is slightly more stable than the low-energy configuration, identified in Sec. III B (the eighth configuration in Table III). We thus propose the 22nd configuration [Fig. 6(a)] as the ground state of $[\text{B}_{12}(\text{CBC})]_{0.67}[\text{B}_{12}(\text{CBCB})]_{0.33}$. In addition, owing to the similarities in terms of superatomic configuration and total energy between the 22nd and 23rd configurations, we presumably infer that the 23rd configuration, constructed within a supercell composed of $4 \times 3 \times 3$ rhombohedral primitive unit cells of boron carbide, is representative of the primitive unit cell of the predicted ground state of $[\text{B}_{12}(\text{CBC})]_{0.67}[\text{B}_{12}(\text{CBCB})]_{0.33}$, as illustrated by Fig. 6(c). We also simulate x-ray powder diffraction patterns of the proposed ground state of $[\text{B}_{12}(\text{CBC})]_{0.67}[\text{B}_{12}(\text{CBCB})]_{0.33}$ (the 23rd configuration), using the RIETAN-FP package [62] as implemented in VESTA [63], and provide it as a fingerprint

for future experimental investigations of boron carbide. The files, containing structural information of the proposed ground state in the VASP format and its simulated powder diffraction patterns are provided as Supplemental Material [64].

Furthermore, by inspecting the configurational specific heat of $[B_{12}(CBC)]_{0.67}[B_{12}(CBCB)]_{0.33}$, derived from the total energy as a function of temperature, we observe a configurational phase transition, taking place at 1700 K. For comparison, the mean-field estimated order-disorder transition temperature, based on the energy difference between the proposed ground state and the ideally random alloy—namely, the 23rd and 19th configurations, listed in Table III, respectively—is 2212 K. The mean-field transition temperature is thus an overestimation of the transition temperature predicted by the MC simulations by $\sim 30\%$. Such an overestimation of the mean-field method is attributed to an absence of the short-range order effects for the disordered configuration of $[B_{12}(CBC)]_{0.67}[B_{12}(CBCB)]_{0.33}$ [18,20,21].

We have, in this section, demonstrated how the cluster expansion approach is employed, together with the MC simulations, to investigate the influence of configuration at the superatomic level on phase stability of boron carbide, in particular $[B_{12}(CBC)]_{0.67}[B_{12}(CBCB)]_{0.33}$. We note that the approach is in principle not restricted either to any specific superatomic formulas or to any specific carbon content of boron carbide within the single-phase region. However, one should be cautious of cases in which various superatomic species are required to describe the configuration of boron carbide. Definitely, this will lead to cumbersome problems of multicomponent systems. The Connolly-Williams cluster expansion approach [36] itself has also drawbacks. That is, one never knows what specific configurations as well as to what range of ECIs should be included in the expansion, i.e., Eq. (5). Given the fact that the ECIs are not restricted by any *a priori* known information, the total energy $E^{\gamma-CE}$ can in principle be identically reproduced by different sets of ECIs. This has a direct impact on the predictive power of the cluster expansion. Additionally, in our case of $[B_{12}(CBC)]_{0.67}[B_{12}(CBCB)]_{0.33}$, the problem has been taken care of at the superatomic level, where configurational disorder of B and C atoms within the superatoms is completely neglected. In reality, such a phenomenon can be thermally induced and should thus be considered for a complete description of the atomic configuration of boron carbide at elevated temperature.

IV. CONCLUSION

We perform first-principles calculations to investigate the phase stability, as well as electronic and elastic properties

of boron carbide. The structural models of boron carbide of different compositions, ranging from $B_{10.5}C$ to B_4C , are constructed using the combination of four structural motifs, recently proposed in the literature [33–35], i.e., $B_{11}C^p(CBC)$, $B_{12}(CBC)$, $B_{12}(CBCB)$, and $B_{12}(B_4)$. We find that $B_{12}(CBCB)$ and $B_{12}(B_4)$ are capable of compensating the electron deficiency in $B_{12}(CBC)$ and they can result in low-energy electron precise configurations.

In the present case, we identify two low-energy configurations at the compositions of $B_{6.67}C$ and $B_{10.5}C$, represented, respectively, by $[B_{12}(CBC)]_{0.67}[B_{12}(CBCB)]_{0.33}$ and $[B_{12}(CBC)]_{0.67}[B_{12}(B_4)]_{0.33}$. Together with the frequently studied $B_{11}C^p(CBC)$ at the composition of B_4C , these three configurations lead to a revolution of the B-C convex hull. As a consequence, $B_{6.5}C$, represented by the electron deficient $B_{12}(CBC)$ and previously proposed in the literature as a stable composition of boron carbide, is no longer part of the B-C convex hull.

Through inspections of the electronic density of states as well as the elastic moduli, we observe that boron carbide, of which the electron deficiency in $B_{12}(CBC)$ is entirely compensated either by $B_{12}(CBCB)$ or by $B_{12}(B_4)$, provides a description for electronic and elastic properties of the material, in agreement with the experimental observations. These results confirm the findings recently reported in Refs. [33–35]. We thus highlight the importance of considering $B_{12}(CBCB)$ and $B_{12}(B_4)$, as well as the previously proposed $B_{11}C^p(CBC)$ and $B_{12}(CBC)$ in their electron precise compositions, as the crucial ingredients for modeling boron carbide with compositions throughout the single-phase region.

ACKNOWLEDGMENTS

Financial support by the Swedish Research Council (VR) through the international career grant No. 2014-6336, Marie Skłodowska Curie Actions, Cofund, Project INCA 600398, and the Swedish Foundation for Strategic Research (SSF) through the Future Research Leaders 6 program is gratefully acknowledged by B.A. S.I.S. acknowledges the Swedish Research Council (VR) Project No. 2014-4750. B.A. and S.I.S. acknowledge the support from the Swedish Government Strategic Research Area in Materials Science on Functional Materials at Linköping University (Faculty Grant SFO-Mat-LiU No. 2009 00971). The simulations were carried out using supercomputer resources provided by the Swedish National Infrastructure for Computing (SNIC) performed at the National Supercomputer Centre (NSC) and the Center for High Performance Computing (PDC). K. Rasim is acknowledged by A.E. for scientifically fruitful discussions.

-
- [1] F. Thevénot, Boron carbide - A comprehensive review, *J. Eur. Ceram. Soc.* **6**, 205 (1990).
 - [2] D. Emin, Unusual properties of icosahedral boron-rich solids, *J. Solid State Chem.* **179**, 2791 (2006).
 - [3] D. Emin, Icosahedral boron-rich solids, *Phys. Today* **40**(1), 55 (1987).
 - [4] J. E. Zorzi, C. A. Perottoni, and J. A. H. da Jornada, Hardness and wear resistance of B_4C ceramics prepared with several additives, *Mater. Lett.* **59**, 2932 (2005).
 - [5] H. Werheit, Boron-rich solids: A chance for high-efficiency high-temperature thermoelectric energy conversion, *Mater. Sci. Eng., B* **29**, 228 (1995).
 - [6] T. L. Aselage, D. Emin, C. Wood, I. Mackinnon, and I. Howard, Anomalous Seebeck coefficient in boron carbides, *MRS Proc.* **97**, 27 (1987).
 - [7] V. Domnich, S. Reynaud, R. A. Haber, and M. Chhowalla, Boron carbide: Structure, properties, and stability under stress, *J. Am. Ceram. Soc.* **94**, 3605 (2011).

- [8] H. K. Clark and J. L. Hoard, The crystal structure of boron carbide, *J. Am. Chem. Soc.* **65**, 2115 (1943).
- [9] H. L. Yakel, The crystal structure of a boron-rich boron carbide, *Acta Crystallogr., Sect. B* **31**, 1797 (1975).
- [10] B. Morosin, A. W. Mullendore, D. Emin, and G. A. Slack, *Rhombohedral Crystal Structure of Compounds Containing Boron-rich Icosahedra*, AIP Conf. Proc. No. 140 (AIP, New York, 1986), p. 70.
- [11] B. Morosin, G. H. Kwei, A. C. Lawson, T. L. Aselage, and D. Emin, Neutron powder diffraction refinement of boron carbides. Nature of intericosahedral chains, *J. Alloys Compd.* **226**, 121 (1995).
- [12] H. Okamoto, B-C (boron-carbon), *J. Phase Equilib.* **13**, 436 (1992).
- [13] I. Jiménez, D. G. Sutherland, T. van Buuren, J. A. Carlisle, L. J. Terminello, and F. J. Himpsel, Photoemission and x-ray absorption study of boron carbide and its surface thermal stability, *Phys. Rev. B* **57**, 13167 (1998).
- [14] V. F. Sears, Neutron scattering lengths and cross sections, *Neutron News* **3**, 26 (1992).
- [15] A. Hushur, M. H. Manghnani, H. Werheit, P. Dera, and Q. Williams, High-pressure phase transition makes $B_{4.3}C$ boron carbide a wide-gap semiconductor, *J. Phys.: Condens. Matter* **28**, 045403 (2016).
- [16] A. Ektarawong, S. I. Simak, and B. Alling, Carbon-rich icosahedral boron carbides beyond B_4C and their thermodynamic stabilities at high temperature and pressure from first principles, *Phys. Rev. B* **94**, 054104 (2016).
- [17] A. Jay, Ph.D. thesis, Ecole Doctorale Polytechnique, 2015.
- [18] S. Yao, W. P. Huhn, and M. Widom, Phase transitions of boron carbide: Pair interaction model of high carbon limit, *Solid State Sci.* **47**, 21 (2015).
- [19] S. Yao, Q. Gao, and M. Widom, Phase diagram of boron carbide with variable carbon composition, *Phys. Rev. B* **95**, 054101 (2017).
- [20] A. Ektarawong, S. I. Simak, L. Hultman, J. Birch, and B. Alling, First-principles study of configurational disorder in B_4C using a superatom-special quasirandom structure method, *Phys. Rev. B* **90**, 024204 (2014).
- [21] A. Ektarawong, S. I. Simak, L. Hultman, J. Birch, and B. Alling, Configurational order-disorder induced metal-nonmetal transition in $B_{13}C_2$ studied with first-principles superatom-special quasirandom structure method, *Phys. Rev. B* **92**, 014202 (2015).
- [22] D. M. Bylander, L. Kleinman, and S. Lee, Self-consistent calculations of the energy bands and bonding properties of $B_{12}C_3$, *Phys. Rev. B* **42**, 1394 (1990).
- [23] S. Aydin and M. Simsek, Hypothetically superhard boron carbide structures with a $B_{11}C$ icosahedral and three-atom chain, *Phys. Status Solidi B* **246**, 62 (2009).
- [24] M. Widom and W. P. Huhn, Prediction of orientational phase transition in boron carbide, *Solid State Sci.* **14**, 1648 (2012).
- [25] D. M. Bylander and L. Kleinman, Structure of $B_{13}C_2$, *Phys. Rev. B* **43**, 1487 (1991).
- [26] J. E. Saal, S. Shang, and Z. K. Liu, The structural evolution of boron carbide via *ab initio* calculations, *Appl. Phys. Lett.* **91**, 231915 (2007).
- [27] N. Vast, J. Sjakste, and E. Betranhandy, Boron carbides from first principles, *J. Phys. Conf. Ser.* **176**, 012002 (2009).
- [28] C. Wood and D. Emin, Conduction mechanism in boron carbide, *Phys. Rev. B* **29**, 4582 (1984).
- [29] L. Zuppiroli, N. Papandreou, and R. Kormann, The dielectric response of boron carbide due to hopping conduction, *J. Appl. Phys.* **70**, 246 (1991).
- [30] M. Calandra, N. Vast, and F. Mauri, Superconductivity from doping boron icosahedra, *Phys. Rev. B* **69**, 224505 (2004).
- [31] D. R. Armstrong, J. Bolland, P. G. Perkins, G. Will, and A. Kirfel, The nature of the chemical bonding in boron carbide. IV. Electronic band structure of boron carbide, $B_{13}C_2$, and the model of the structure $B_{12}C_3$, *Acta Crystallogr., Sect. B* **39**, 324 (1983).
- [32] A. Ektarawong, S. I. Simak, L. Hultman, J. Birch, F. Tasnádi, F. Wang, and B. Alling, Effects of configurational disorder on the elastic properties of icosahedral boron-rich alloys based on B_6O , $B_{13}C_2$, and B_4C , and their mixing thermodynamics, *J. Chem. Phys.* **144**, 134503 (2016).
- [33] K. Shirai, K. Sakuma, and N. Uemura, Theoretical study of the structure of boron carbide $B_{13}C_2$, *Phys. Rev. B* **90**, 064109 (2014).
- [34] K. Rasim, R. Ramlau, A. Leithe-Jasper, T. Mori, U. Burkhardt, H. Borrmann, W. Schnelle, C. Carbogno, M. Scheffler, and Y. Grin, Local Atomic Arrangements and Band Structure of Boron Carbide, *Angew. Chem.* **130**, 1 (2018).
- [35] K. Rasim, C. Carbogno, R. Ramlau, A. Leithe-Jasper, T. Mori, H. Borrmann, U. Burkhardt, W. Schnelle, M. Scheffler, and Y. Grin, A comprehensive study of intrinsic defects in boron carbide, *19th International Symposium on Boron, Borides and Related Materials (ISBB)* (Freiburg, Germany, 2017); K. Rasim, C. Carbogno, and Y. Grin, Intrinsic defects in boron carbide - a comprehensive first-principles study (unpublished).
- [36] J. W. D. Connolly and A. R. Williams, Density-functional theory applied to phase transformations in transition-metal alloys, *Phys. Rev. B* **27**, 5169(R) (1983).
- [37] P. E. Blöchl, Projector augmented-wave method, *Phys. Rev. B* **50**, 17953 (1994).
- [38] G. Kresse and J. Furthmüller, Efficiency of *ab-initio* total energy calculations for metals and semiconductors using a plane-wave basis set, *Comput. Mater. Sci.* **6**, 15 (1996).
- [39] G. Kresse and J. Furthmüller, Efficient iterative schemes for *ab initio* total-energy calculations using a plane-wave basis set, *Phys. Rev. B* **54**, 11169 (1996).
- [40] J. Perdew, K. Burke, and M. Ernzerhof, Generalized Gradient Approximation Made Simple, *Phys. Rev. Lett.* **77**, 3865 (1996).
- [41] H. J. Monkhorst and J. D. Pack, Special points for Brillouin-zone integrations, *Phys. Rev. B* **13**, 5188 (1976).
- [42] P. E. Blöchl, O. Jepsen, and O. K. Andersen, Improved tetrahedron method for Brillouin-zone integrations, *Phys. Rev. B* **49**, 16223 (1994).
- [43] A. Zunger, S.-H. Wei, L. G. Ferreira, and J. E. Bernard, Special Quasirandom Structures, *Phys. Rev. Lett.* **65**, 353 (1990).
- [44] R. Golezorkhtabar, P. Pavone, J. Spitaler, P. Puschnig, and C. Draxl, ElaStic: A tool for calculating second-order elastic constants from first principles, *Comput. Phys. Commun.* **184**, 1861 (2013).
- [45] F. Tasnádi, M. Odén, and I. A. Abrikosov, *Ab initio* elastic tensor of cubic $Ti_{0.5}Al_{0.5}N$ alloys: Dependence of elastic constants on size and shape of the supercell model and their convergence, *Phys. Rev. B* **85**, 144112 (2012).

- [46] J. F. Nye, *Physical Properties of Crystals: Their Representation by Tensors and Matrices* (Oxford University Press, New York, 1985).
- [47] L. Vitos, *Computational Quantum Mechanics for Materials Engineers: The EMTO Method and Applications (Engineering Materials and Processes)* (Springer, Berlin, 2010).
- [48] M. Moakher and A. N. Norris, The closest elastic tensor of arbitrary symmetry to an elasticity tensor of lower symmetry, *J. Elast.* **85**, 215 (2006).
- [49] G. Simmons and H. Wang, *Single Crystal Elastic Constants and Calculated Aggregate Properties: A Handbook* (MIT Press, Cambridge, MA, 1971).
- [50] H. C. Longuet-Higgins and M. de V. Roberts, The electronic structure of an icosahedron of boron atoms, *Proc. R. Soc. A* **230**, 110 (1955).
- [51] C. Pallier, J.-M. Leyssale, L. A. Truffandier, A. T. Bui, P. Weisbecker, C. Gervais, H. E. Fischer, F. Sirotti, F. Teyssandier, and G. Chollon, Structure of an Amorphous Boron Carbide Film: An Experimental and Computational Approach, *Chem. Mater.* **25**, 2618 (2013).
- [52] J. K. Sonber, T. S. R. Ch. Murthy, C. Subramanian, R. K. Fotedar, R. C. Hubli, and A. K. Suri, Synthesis, densification and characterization of boron carbide, *Trans. Ind. Ceram. Soc.* **72**, 100 (2013).
- [53] J. H. Gieske, T. L. Aselage, and D. Emin, *Elastic Properties of Boron Carbides*, AIP Conf. Proc. No. 231 (AIP, New York, 1991), p. 376.
- [54] M. H. Manghnani, Y. Wang, F. Li, P. Zinin, and W. Rafaniello, Elastic and vibrational properties of B_4C to 21 GPa, *Proceedings of the International Conference on High Pressure Science and Technology*, AIRAPT-17, edited by R. M. Hazen and R. T. Downs (Universities Press, India, 2000).
- [55] H. Werheit, H. Binnenbruck, and A. Hausen, Optical properties of boron carbide and comparison with β -rhombohedral boron, *Phys. Status Solidi B* **47**, 153 (1971).
- [56] H. Werheit, M. Laux, U. Kuhlmann, and R. Telle, Optical interband transitions of boron carbide, *Phys. Status Solidi B* **172**, K81 (1991).
- [57] H. Werheit, C. Janowitz, R. Schmechel, T. Tanaka, and Y. Ishizawa, Interband critical points of some icosahedral boron-rich solids, *J. Solid State Chem.* **133**, 132 (1997).
- [58] H. Werheit, On excitons and other gap states in boron carbide, *J. Phys.: Condens. Matter* **18**, 10655 (2006).
- [59] C. He and J. X. Zhong, Structure, stability, mechanical and electronic properties of α -boron and α^* -boron, *AIP Adv.* **3**, 042138 (2013).
- [60] C. Cheng, K. M. Reddy, A. Hirata, T. Fujita, and M. Chen, Structure and mechanical properties of boron-rich boron carbides, *J. Eur. Ceram. Soc.* **37**, 4514 (2017).
- [61] N. Metropolis, A. W. Rosenbluth, M. N. Rosenbluth, A. H. Teller, and E. Teller, Equation of state calculations by fast computing machines, *J. Chem. Phys.* **21**, 1087 (1953).
- [62] F. Izumi and K. Momma, Three-dimensional visualization in powder diffraction, *Solid State Phenom.* **130**, 15 (2007).
- [63] K. Momma and F. Izumi, VESTA3 for three-dimensional visualization of crystal, volumetric and morphology data, *J. Appl. Crystallogr.* **44**, 1272 (2011).
- [64] See Supplemental Material at <http://link.aps.org/supplemental/10.1103/PhysRevB.97.174104> for the files containing structural information of the proposed ground-state configuration of $[B_{12}(CBC)]_{0.67}[B_{12}(CBCB)]_{0.33}$ (Fig. 6) and its simulated x-ray powder diffraction patterns.